RSC Advances

ROYAL SOCIETY OF CHEMISTRY

www.rsc.org/advances

Cite this: DOI: 10.1039/c0xx00000x

www.rsc.org/xxxxxx

ARTICLE TYPE

Power-output Reduction of Graphene Oxide and MnO_2-free Zn/GO Primary Cell

Wufeng Chen, Xiayu Feng, Junhao Chen and Lifeng Yan*

Received (in XXX, XXX) Xth XXXXXXXXX 20XX, Accepted Xth XXXXXXXXX 20XX
DOI: 10.1039/b000000x

The reduction of graphene oxide (GO) by zinc powder is an electron-input process essentially. Is it possible to output the electron during the reduction for a primary battery? Here, a primary battery of Zn plate as anode and the centimeter-sized dried foam film of graphene oxide (GO) as cathode has been fabricated, and the electron-output has been achieved while a reduced graphene oxided film was obtained synchronously. The output capacity of the batteries depends on the oxygenated degree and the amount of GO, and the maximum specific capacity is 642 mAh g^{-1} while the average voltage is up 0.6 V. Electrochemical impedance spectroscopy (EIS) measurements revealed the decreasing resistance of Zn/GO cell during discharging process. A LED lamp can be ignited by the battery, indicating its potential for practical application. In addition, the primary battery is MnO_2-free, is more environmentally benign than the traditional Zn/Carbon dry batteries.

Introduction

Since the obtaining of a single layer structure in 2004,[1] graphene, the thinnest carbon material, has attracted gigantic attention for its potential application in many fields.[2-7] Batteries are the major applied fields while graphene has been used as materials for electrodes dues to its high electrical conductivity and surface area.[8-11] As a basic, the preparation of graphene or reduced graphene oxide (rGO) is still a challenge, especially in large scale.[12] Chemical reductions of graphene oxide (GO) are a major route to prepare rGO, and various kinds of reduction agents or methods had been reported.[13] Among them, metals, such as Zn, Al, Fe etc. had been used as reducing agent for rGO preparation using GO as feedstock.[14-18] Mechanism studies revealed that the driving force of the reduction comes from the releasing of electrons of metal to GO sheets while the metal was oxidized. The acceptance of electron of GO under acidic condition will help to remove the oxygen-containing groups in GO, and results in the formation of rGO.[15] Similar processes can also be found in the electrochemical reduction of GO to rGO, where GO nanosheets are directly coated on the surface of electrodes during electron injection, and the process is a typical electrolysis with consumption of electric energy.[19, 20] Is it possible to output the power during the reduction of GO?

Primary cell or battery is the ideal device for power-output, and usually the metal works as the anode, such as Zn/carbon cell, which has been widely used as dry batteries in our daily application.[21, 22] Typically, in this process, metal of anode lost electrons while it was oxidized to form metal ions diffusion into the electrolyte and the electrons were output by a conducting wire to electrical devices, and then the electrons were injected into the cathode to reduce the cathode materials.Similarly, the reduction of GO by metals can be used to design a primary cell where metal (Zn plate) works as the anode and GO works as the cathode (Fig.1a). Power-output can be achieved by using an exterior passageway to export electrons while the GO can be reduced at the cathode, playing a role of depolarizer, and the as formed rGO directly works as the current collector and cathode. In the process, aqueous of NH_4Cl or KOH are used as electrolytes. In addition, in a typical Zn/C cell, MnO_2 with Hg is usually employed as the cathode materials, where MnO_2 and Hg are the source of metal pollution during the disposition of waste batteries.[23, 24] So, MnO_2-free cell will be attracting for its environmentally benign properties. Here, in the design of new cell, GO will replace of MnO_2, and the next generation of MnO_2-free cell is the target.

Here, a free-standing film of GO was directly employed as the cathode in an antitype of the Zn/GO cell, and a powder-output primary cell has been fabricated.

Experimental Materials

Graphite powder, 100mesh, 99.9% (metals basis) acetylene was purchased from Alfa Aesar. 60% PTFE was purchased from Aladin. Analytical grade $NaNO_3$, P_2O_5, $ZnCl_2$, NH_4Cl, $KClO_3$, KOH, $KMnO_4$, 98% H_2SO_4, 30% H_2O_2 aqueous solution, Zinc plate were purchased from Shanghai Chemical Reagents Company, and were used directly without further purification. Ultra-pure water (18 MΩ) was produced by a Millipore System (Millipore Q, USA). Chlorosulfonic acid ($ClSO_3H$) was purchased from Graxia Chemical Technology Co., Ltd. Electrolytically precipitated, Manganese(IV) Oxide, 88%, was purchased from Alfa Aesar.

Preparation of GO

600mg graphite powder (100 mesh) was immersed with 6.0 ml chlorosulfonic acid in a Teflon reactor at 150 ^oC for 12h, and the

mixture was transferred in a 250ml beaker after adding of 15.0 ml H_2SO_4 and 1.0 g P_2O_5. Then 8.0 ml 30% H_2O_2 was added into acidic mixture slowly. Next, 200.0 ml DI water was added to wash the sample, and expanded graphite powder was collected by filtration and freeze-drying. The expanded graphite was employed as raw material for oxidation to prepare graphene oxide, and the expanded graphite prepared by rapid thermal expansion method can also be used as feedstock as well. For the GO preparation, modified Brodie method was employed [25], 0.2 g expanded graphite was mixed with 16.0 ml 98% H_2SO_4, 3.0 ml concentrated nitric acid and specific amount of $KClO_3$, and the reaction process lasted for 4 days at 30 ^oC. The amount of $KClO_3$ was 1.0 g, 1.6 g and 2.2 g for GO-1, GO-3 and GO-4 respectively. Then the sediments were collected after centrifugation at 7200rpm for 6 times, final GO powders were obtained after freeze-drying treatment. While thermal treated GO-4 powder at 90 ^oC for 3days was named as GO-2. GO was also prepared by the modified Hummer method using expanded graphite as raw material. Typically, 400 mg expanded graphite was added into a 50 mL beaker and 25.0 mL of H_2SO_4 was added under stirring in an ice-bath. Then specific amount of $KMnO_4$ (1.2g $KMnO_4$ for the moderate oxidation sample and 2.4g$KMnO_4$ for the strong oxidation sample) was added slowly into the beaker under stirring and the temperature of the system was controlled lower than 20 ^oC. Next, the system maintained reaction for 1 day at room temperature, and then 100 mL water was slowly added into the system and it was stirred for another 20min. 80 ml of hot water with 60 ^oC and 3.0% H_2O_2 aqueous solution were added to reduce the residual $KMnO_4$ until the bubbling disappeared. GO was collected by centrifugation at 7200rpm for 6 times. The ultimate GO powder was obtained after freeze-drying treatment.

Preparation of dried GO foam films

First, aqueous solution of GO at 6mg/mL was prepared by dispersing GO in deionized water under mild ultrasound for 15 min, and 0.1v% butylamine was added. Then a cycle of Ag or copper wire was vertically or horizontally dipped into the solution and gently lifted from the solution. A small volume of aqueous solution of GO was captured by the substrates during the process, and the substrates were then allowed to stand in air for hours to dry. Generally, the drying process was carried out at room temperature under normal humidity condition (~20%). For a rapid GO foam film fabrication, it can also be dried in warm air of about 60 ^oC.

Fabrication of Zn-GO primary cell

For the antetype cell, the dried foam film was directly used as the cathode, and zinc plate was used as anode while NH_4Cl worked as electrolyte. While nickel foam as current collector for GO cathode, 15mg GO was deposited on it without any addition. If the powder of GO was used as the active electrode material, cathode was prepared by mixing GO, PTFE and acetylene with amount ratio of 7:2:1, carbon felt or foam nickel was employed as anodic collector while NH_4Cl or KOH aqueous solutions were used as electrolytes, respectively. Zinc plate (1.5 cm×2.0 cm×0.1 cm) was employed as the anode material, and cellulose filter was employed as cell membrane. Generally, the NH_4Cl electrolyte was composed of 4.0 M NH_4Cl, 1.0M $ZnCl_2$, and small amount of $BiCl_3$, while the alkaline electrolyte was composed of 5.0 M KOH.

Electrochemical characterization

Cyclic voltammetry (CV), electrochemical impedance spectroscopy (EIS) measurements and galvanostatic discharge experiments were performed on a CHI660C potentiostat-galvanostat (CH Instruments Inc.). For EIS measurement, the ac frequency range was from 0.01 to 10^5 Hz with an AC amplitude of 5 mV. For CV analysis, 5.0 M KOH was placed in an electrochemical cell as electrolyte, which included a piece of nickel foam containing 1mg active material (working electrode), a platinum wire (counter electrode) and an Hg/Hg_2Cl_2 reference electrode. CV tests were carried out at a scan rate of 0.5mV s^{-1} and over a potential range of 0 to 0.9 V (vs. SCE). To collect the rGO after discharge without impurity for experimental analysis, GO was deposited in nickel foam without additional PTFE and acetylene, end voltage was 0.6V and 0.25V for 0.6Vdischarged GO and fully discharged GO respectively. After discharge, rGO powder was collected by ultrasound and washed with HCl(1M) aqueous and water before drying.

Characterization

Wide-angle X-ray diffraction (XRD) analyses were carried out on an X-ray diffractometer (D/MAX-1200, Rigaku Denki Co. Ltd., Japan). The XRD patterns with Cu Ka radiation (λ= 1.5406) at 40 kV and 100 mA were recorded in the range of 2θ = 5-65°. A commercial atomic force microscope (AFM, Nanoscope IIIa; Digital Instruments, Santa Barbra, CA), equipped with a J scanner was used to measure the morphologies and thicknesses of the samples. Si_3N_4 tip (Nanoprobes, Digital Instruments Inc.) was used by the contact mode. The scan rates were between 1.0 and 2.4 Hz. X-ray photoelectron spectroscopy (XPS) were recorded on an Escalab MK II photoelectron spectrometer (VG Scientific Ltd., United Kingdom). Raman spectra was taken on a RAMAMLOG 6 (Spex, USA) using a 50× objective lens with a 514.5 nm laser excitation. The structures of the films were measured using a Sirion 200 FESEM at an accelerating voltage of 10 kV. Elemental analysis was carried out by a VARIO ELIII analyzer (Elemental Co., Germany). The optical images of the film formation were determined by optical microscopy (POM) (LW200-PC, Cewei, Shanghai) using a 40× objective lens at room temperature.

Results and Discussion

In our previous study, we found that it is easy to prepare centimeter-size free-standing ultrathin dried foam film of GO by a novel bobble film technique with a metal frame,[26] and here, a copper rectangular frame was used to prepare a free-standing film of GO, as shown in Fig.1b-c, the as-prepared free-standing GO film was transparent with 1.5 cm in width and 3.1 cm in length, and it was directly used as the cathode while a Zn plate worked as the anode and NH_4Cl as electrolyte for the Zn/GO cell. Once the cell began to work, the transparent GO film became dark from the brim to the interior of the film, and at the end of the GO film

became dark completely, indicating the efficient reduction of GO film to rGO film. Notably, during the process we did not observe the hydrogen bubbles occurred from cathode, demonstrating the effective electron capture ability of GO.

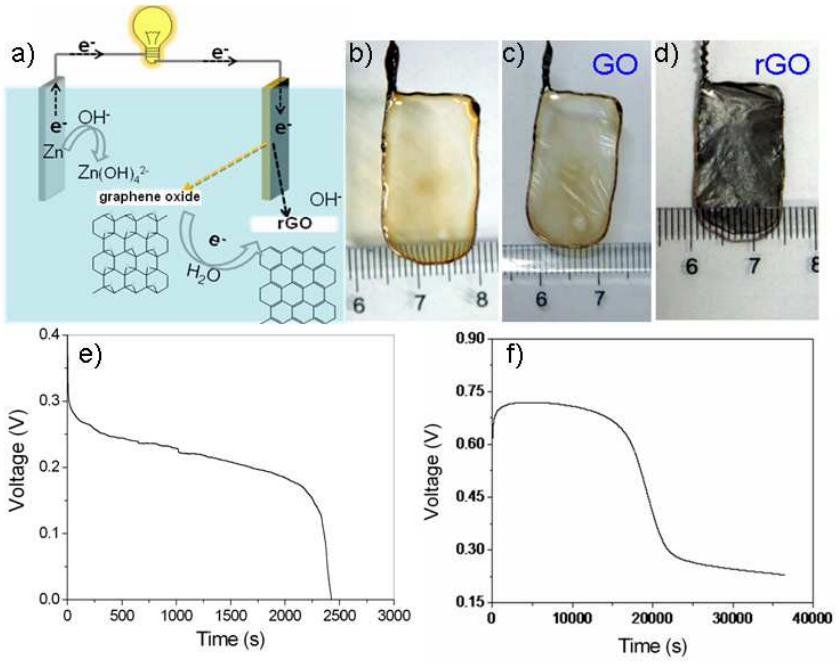

Figure 1. Schematic diagram showing the Zn/GO cell (a), photoimages of the liquid film of GO (b), dried foam film of GO (b), and rGO film formed during work as the cathode of the Zn/GO cell (d), and discharge curve of the Zn/GO primary cell with Zinc plate as anode and the dried foam film of GO as the cathode (e) or with GO deposited on nickel foam as anode (f). Both were carried out in KOH electrolyte at 1.5mA.

Figure 1e and f show the discharge performance of a Zn/GO cell using the above rGO film as the cathode, and the discharge current density is 1.5 mA. The cell voltage is about 0.3 V at the beginning, and decreases slowly to about 0.18 V at 2100 s, and then quickly decreases to zero at time of 2400 s. Before 2100 s, the cell works normally with the reduction of the GO film by electrons, and at the end no more GO can be reduced by the process, and the cell is fully discharged while a black rGO film (Fig.1c) was obtained. The discharge reaction of the Zn/GO primary cell can be described as:

$$\text{Anode: } Zn + 4OH^- \rightarrow [Zn(OH)_4]^{2-} + 2e$$

$$\text{Cathode: } GO + 2e + 2H^+ \rightarrow rGO + H_2O$$

The foam film was limited by its centimeter scale size, for a larger scale reduction of GO by discharging process. GO was deposited on nickel foam, which could act as a current collector. Improved conductivity of the working electrode resulted in a higher working voltage over 0.6V.

Table 1. Capacity, average working voltage and energy density of cathode materials in primary cells.

	MnO_2	MnO_2	GO-1	GO-2	GO-3	GO-4	GO-ideal
Formula	MnO_2	MnO_2	$C_2O_{0.62}H_{0.66}$	$C_2O_{0.96}H_{0.90}$	$C_2O_{1.18}H_{1.05}$	$C_2O_{1.44}H_{1.13}$	C_2O
Electrolyte	KOH	NH_4Cl	NH_4Cl	NH_4Cl	NH_4Cl	NH_4Cl	\
Capacity (mAh g^{-1})	237	206	216	610	642	505	1340
Voltage (V)	1.15	1.19	0.94	0.76	0.68	0.88	\
E (Wh kg^{-1})	272	245	204	466	440	445	\

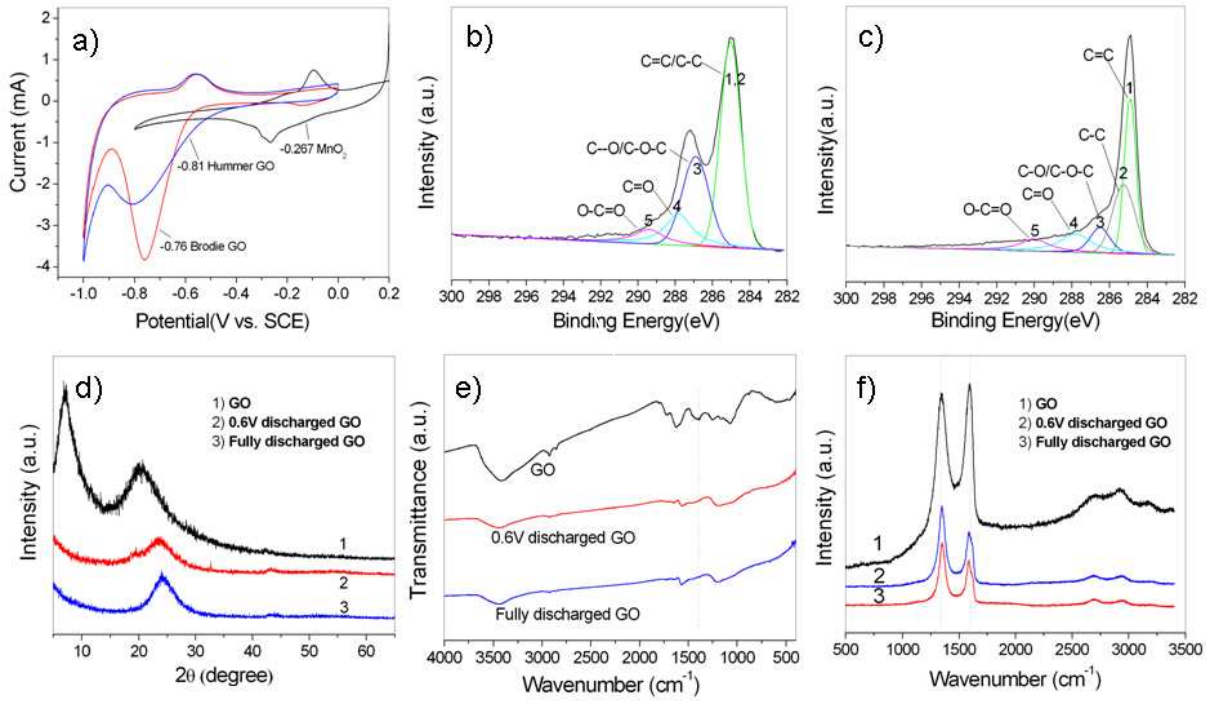

Figure 2. Cyclic voltammetry analysis of different cathode materials at 0.5mv s^{-1}, three electrode system, nickel foam as current collector of working electrode (a); XPS profiles of the GO (b) and rGO (c) after the cell was fully discharged; XRD (d), FT-IR (e), and Raman (f) spectra of GO and rGO formed at 0.6V or fully discharged.

Figure 2a shows the cyclic voltammograms of MnO_2 and GO prepared by Hummer or Brodie methods respectively, and the scan rate is 0.5 mV s^{-1} with KOH as the electrolyte. For MnO_2, the reduction peak and oxidation peak both appear, and the reduction peak is at -0.267 V. However, for Brodie GO and Hummer GO, the reduction peaks appear at -0.76 V and -0.81 V, respectively, while the relative chemical content of them are $C_2O_{1.18}H_{1.05}$ and $C_2O_{1.32}H_{1.06}$, indicating the lower working voltage of GO than that of MnO_2.

XPS measurements could provide the direct evidence of the reduction of GO. Figure 2b and c show the C_{1s} XPS spectra of both the Brodie GO and as-formed rGO after the cell fully discharged. Both the curves were fitted considering the following contributions: C=C (sp^2; peak 1), C-C (sp^3; peak 2), C-O/C-O-C (hydroxyl and epoxy groups; peak 3), C=O (carbonyl groups; peak 4), O-C=O (carboxyl groups; peak 5).[27] Figure 2b also shows the C_{1s} peaks of GO, which consists of three main components arising from C-O (hydroxyl and epoxy, 286.9 eV), C=O (carbonyl, 287.8 eV) and C=C/C-C (284.9 eV) species, and a minor component of O=C-O (carboxyl, 289.5 eV) species. After reduction by the fully discharge, the oxygen species of C-O (hydroxyl and epoxy, 286.9 eV), C=O (carbonyl, 287.8 eV) and O=C-O (carboxyl, 289.5 eV) reduced significantly as shown in Figure 2c, indicating an efficient deoxidization. The major species remaining were C=C and C-C. The calculated C/O mole ratio increased from 1.64 to 8.4 after the reduction.

Figure 2d shows the X-ray diffraction (XRD) patterns of GO, rGO obtained after 0.6 V discharge, and fully discharge, respectively. For GO there appears two diffraction peaks at 7.2° and 20.3°, corresponds to a d-spacing of 1.23 and 0.44 nm. After discharge, the diffraction peaks appear at 23.4° and 24.1° for 0.6V discharged and fully discharged rGO, respectively, correspond to the interlayer spacing of 0.38 nm and 0.37 nm, which are still higher than that of pristine graphite (0.34 nm), indicating the packing density of the rGO sheets became higher than that of GO. Figure 2e shows the typical FT-IR spectra of GO and the rGO obtained by 0.6 V or fully discharge respectively. For GO, the characteristic peaks appear for carbonyl C=O (1726 cm^{-1}), aromatic C=C (1570 cm^{-1}), epoxy C–O (1410 cm^{-1}), and C–O (1070 cm^{-1}).[28] After reduction by discharge, the peaks for epoxy functional group were reduced significantly, and the peaks of carboxy and hydroxide groups also decreased observably, indicating the efficient reduction of GO during the process of discharge.

Figure 2f shows the typical Raman spectra of GO and the rGO obtained by 0.6 V or fully discharge respectively. All the spectra indicate the existence of the D, G and 2D bands. For GO, the G band is located at 1595 cm^{-1}, while for the rGO obtained after 0.6V or fully discharge the G band moved to 1588 cm^{-1}, which is close to the value of the pristine graphite and it confirms the reduction of GO during the discharge. However, the existence of the D band at 1341, 1349 and 1353 cm^{-1} corresponding to GO and rGO of 0.6V and fully discharged also predicts the defect of the sample and the size of the in-plane sp2 domain.[29] The intensity ratio of the D and G band (I_D/I_G), varies from 0.96 to 1.33 (for both discharged rGO). The result is quite unexpected and apparently contradicts with the idea that a significant reduced D band should be observed after electrochemical reduction of oxidized graphene. It believes that this contradiction comes from

the amorphous character of GO, for a large distortion of the 6-fold aromatic rings in amorphous carbon, the I_D/I_G ratio decreases rather than increase upon oxidization of this highly defected carbon structure. Thus here, the I_D/I_G ratio cannot be used as a measure of structural disorder and, accordingly, comparisons between materials of amorphous GO and graphitic rGO are no longer valid. Similar results also have been reported by Stankovich et al during chemical reduction process of GO.[30]

The above results reveals that GO can be efficiently reduced when it works as the cathode in the Zn/GO cell. However, the voltage and capacity are still low, indicating the amount of the GO in the cell is insufficient.

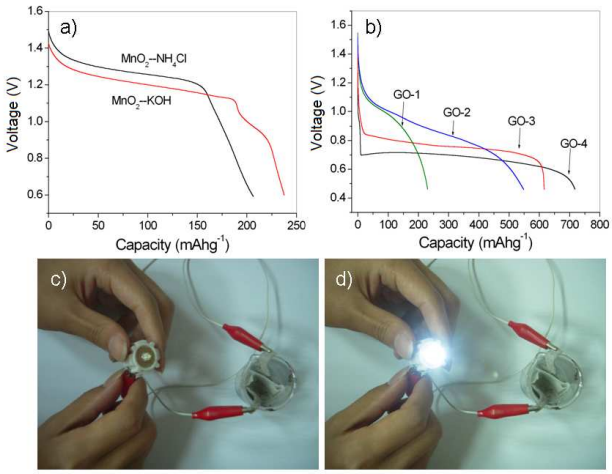

Figure 3. Galvanostatic discharge curves of MnO_2 in NH_4Cl and KOH aqueous electrolytes (a) or GO with different oxidation degrees in NH_4Cl electrolyte at 1.5mAcm^{-2}, respectively (b); Photos of a Zn/GO primary cell before (c) and after (d) the LED lamp was lighten.

Improved conductivity of the electrode and the amount of GO could increase the discharge voltage before it reaches the ideal potential of Zn/GO cell. Here, a new Zn/GO cell was fabricated where the cathode was prepared by mixing of GO powder, PTFE and acetylene with mass ratio of 7:2:1, carbon felt or foam nickel were employed as anodic collectors while NH_4Cl or KOH aqueous solutions were used as electrolytes, respectively. Zinc plate (1.5cm×2.0cm×0.1cm) was employed as anode, and cellulose filter was employed as a cell membrane. A LED lamp was connected by conductive wire to the anode while the cathode was not connected as shown in Fig.3c, and then both electrodes were connected to let the cell discharge, and the LED lamp was ignited as shown in Fig.3d, indicating the Zn/GO cell can output enough energy for practical applications. Galvanostatic curves of both GO and MnO_2 for Zn/GO or Zn/MnO_2 were measured, respectively. Figure 3a shows the curve of MnO_2 in NH_4Cl or KOH electrolytes at 1.5 mAcm^{-2}, and discharge capacities are 237 mAhg^{-1} and 206 mAhg^{-1} respectively when the discharge voltage is up to 0.6V. For GO, the galvanostatic curves strongly depend on the formula of the GO, as shown in Fig.3b, for GO-1, the discharge capacity is only about 200 mAhg^{-1}, while for GO-4, the maximal capacity is 642 mAhg^{-1}, and this value can expand to 705 mAhg^{-1} if 0.5V is the end voltage. So, the chemical composition of the GO is a key factor, and a series of GO have been tested in NH_4Cl electrolyte, and the results are listed in Table 1. Clearly, the larger the oxygen content GO contained, the bigger capacity the cell output. To further clarify the relationship between oxidization degree and capacity of the GO, theoretical columbic capacity of 662 mAh g^{-1} was calculated according the components change from GO to rGO, $C_2O_{1.18}H_{1.05}$ for GO as cathode material, and $C_2O_{0.344}H_{0.458}$ for the discharged rGO. Both were measured by elementary analysis. The working capacity of the corresponding cell was measured at 642 mAh g^{-1}, 92% of theoretical value. This shows high relativity between the oxidization degree and capacity of the GO.

What happened to GO during the discharge process? Here, the discharging process of GO dried foam film was directly observed under a microscope during the discharge (Fig.4a), and the GO dried foam film was made according to our previous method [31], with silver wire as the conductive frame. At the beginning of discharge, the transparent GO film turned into black at the edge, indicating the reduction of GO to rGO (Fig.4c). Then, the process continued with the black region diffusing into the center of the film until the whole film became black (Fig.4d-g), indicating the full discharge of the cell. This process also can be described as a Domino process as shown in Fig.4b, and the graphene oxide sheet near silver frame captured electron firstly and was reduced into rGO. Then the conductive rGO became the new edge for electron transfer, causing the reduction of graphene oxide sheets forward until all the connected graphene oxide sheets were reduced. This also made GO electrode smooth discharging process and better conductivity property than that of MnO_2, as shown in the EIS studies of cells (Fig.S4).

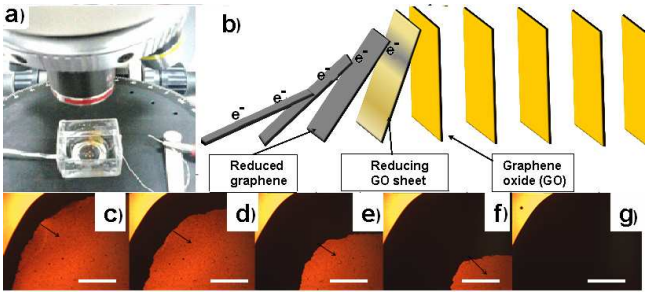

Figure 4. a)In-situ observation of the discharging process of GO dried foam film immersed in NH_4Cl electrolyte as cathode while zinc as anode, magnification at 40. c-g) color changes of the GO film during discharging processing, scale bar 1mm. b) Domino-like reduction of GO nanosheets inside the film during discharging.

Conclusions

In summary, A power-output type reduction of GO has been developed, where the dried foam film of GO was used as cathode and Zinc plate as anode. The discharging process can efficiently reduce GO film to rGO film while electrical energy was output. It was found that the output capacity of the Zn/GO primary cell depends on the oxygen content of the GO sheets, and a maximum of specific capacity of 642 mAh g^{-1} has been achieved when the formula of the GO is $C_2O_{1.18}H_{1.05}$, and the average voltage changed from 0.68 to 0.94 V. Carbonyl and epoxy groups are the main groups contributing to the capacity. Electrochemical impedance spectroscopy (EIS) measurements revealed the decreasing resistance of Zn-GO cell during discharging process. The reduction of the GO film during discharge can be described as a domino-like process. The Zn/GO primary cell has potential

practical application as battery, and a LED lamp can be ignited here. Besides, we also can connect cells in series for higher working voltage and more wide applications.

Acknowledgements

This work is supported by the National Natural Science Foundation of China (No.51373162), the National Basic Research Program of China (No. 2010CB923302 and 2011CB921403), and The USTC Special Grant for Postgraduate Research, Innovation and Practice.

References

Hefei National Laboratory for Physical Sciences at the Microscale and Department of Chemical Physics, University of Science and Technology of China. Hefei, 230026, P.R. China., Fax: +86-551-3603748; Tel:+86-551-63606853; E-mail: lfyan@ustc.edu.cn

1. K. S. Novoselov, A. K. Geim, S. V. Morozov, D. Jiang, Y. Zhang, S. V. Dubonos, I. V. Grigorieva and A. A. Firsov, *Science*, 2004, **306**, 666-669.
2. X. J. Wan, Y. Huang and Y. S. Chen, *Acc. Chem. Res.*, 2012, **45**, 598-607.
3. Y. Zhu, D. K. James and J. M. Tour, *Adv. Mater.*, 2012, **24**, 4924-4955.
4. D. A. C. Brownson, D. K. Kampouris and C. E. Banks, *Chem. Soc. Rev.*, 2012, **41**, 6944-6976.
5. Y. Chen, B. Zhang, G. Liu, X. D. Zhuang and E. T. Kang, *Chem. Soc. Rev.*, 2012, **41**, 4688-4707.
6. X. Huang, X. Y. Qi, F. Boey and H. Zhang, *Chem. Soc. Rev.*, 2012, **41**, 666-686.
7. K. P. Loh, Q. L. Bao, G. Eda and M. Chhowalla, *Nature Chemistry*, 2010, **2**, 1015-1024.
8. L. M. Dai, *Acc. Chem. Res.*, 2013, **46**, 31-42.
9. X. Huang, Z. Y. Zeng, Z. X. Fan, J. Q. Liu and H. Zhang, *Adv. Mater.*, 2012, **24**, 5979-6004.
10. Y. Q. Sun, Q. O. Wu and G. Q. Shi, *Energy & Environmental Science*, 2011, **4**, 1113-1132.
11. C. H. Xu, B. H. Xu, Y. Gu, Z. G. Xiong, J. Sun and X. S. Zhao, *Energy & Environmental Science*, 2013, **6**, 1388-1414.
12. C. K. Chua and M. Pumera, *Chem. Soc. Rev.*, 2014, **43**, 291-312.
13. T. Kuila, A. K. Mishra, P. Khanra, N. H. Kim and J. H. Lee, *Nanoscale*, 2013, **5**, 52-71.
14. N. H. Kim, P. Khanra, T. Kuila, D. Jung and J. H. Lee, *Journal of Materials Chemistry A*, 2013, **1**, 11320-11328.
15. S. Yang, W. B. Yue, D. Z. Huang, C. F. Chen, H. Lin and X. J. Yang, *Rsc Advances*, 2012, **2**, 8827-8832.
16. R. S. Dey, S. Hajra, R. K. Sahu, C. R. Raj and M. K. Panigrahi, *Chem. Commun.*, 2012, **48**, 1787-1789.
17. S. Sarkar and D. Basak, *Chem. Phys. Lett.*, 2013, **561**, 125-130.
18. X. G. Mei and J. Y. Ouyang, *Carbon*, 2011, **49**, 5389-5397.
19. Y. Y. Shao, J. Wang, M. Engelhard, C. M. Wang and Y. H. Lin, *J. Mater. Chem.*, 2010, **20**, 743-748.
20. Z. J. Wang, X. Z. Zhou, J. Zhang, F. Boey and H. Zhang, *Journal of Physical Chemistry C*, 2009, **113**, 14071-14075.
21. A. A. El Mel, M. Buffiere, C. P. Ewels, L. Molina-Luna, E. Faulques, J. F. Colomer, H. J. Kleebe, S. Konstantinidis, R. Snyders and C. Bittencourt, *Carbon*, 2014, **66**, 442-449.
22. Z. Q. Wang, N. Bramnik, S. Roy, G. Di Benedetto, J. L. Zunino and S. Mitra, *J. Power Sources*, 2013, **237**, 210-214.
23. S. P. Singh, M. Kumari, S. I. Kumari, M. F. Rahman, M. Mahboob and P. Grover, *J. Appl. Toxicol.*, 2013, **33**, 1165-1179.
24. H. A. Barrett, A. Ferraro, C. Burnette, A. Meyer and M. P. S. Krekeler, *J. Power Sources*, 2012, **206**, 414-420.
25. B. C. Brodie, *Phil. Trans. R. Soc. Lond.*, 1859, **149**, 249-259.
26. W. F. Chen and L. F. Yan, *Adv. Mater.*, 2012, **24**, 6229-6233.
27. S. Hyeon-Jin, K. Ki Kang, A. Benayad, Y. Seon-Mi, P. Hyeon Ki, J. In-Sun, J. Mei Hua, J. Hae-Kyung, K. Jong Min, C. Jae-Young and L. Young Hee, *Advanced Functional Materials*, 2009, 1987-1992.
28. S. Park, J. H. An, R. D. Piner, I. Jung, D. X. Yang, A. Velamakanni, S. T. Nguyen and R. S. Ruoff, *Chemistry of Materials*, 2008, **20**, 6592-6594.
29. J. I. Paredes, S. Villar-Rodil, P. Solis-Fernandez, A. Martinez-Alonso and J. M. D. Tascon, *Langmuir*, 2009, **25**, 5957-5968.
30. S. Stankovich, D. A. Dikin, R. D. Piner, K. A. Kohlhaas, A. Kleinhammes, Y. Jia, Y. Wu, S. T. Nguyen and R. S. Ruoff, *Carbon*, 2007, **45**, 1558-1565.
31. W. Chen and L. Yan, *Advanced Materials*, 2012, **24**, 6229-6233.

Power-output Reduction of Graphene Oxide and MnO_2-free Zn/GO Primary Cell

Wufeng Chen, Xiayu Feng, Junhao Chen, Lifeng Yan*

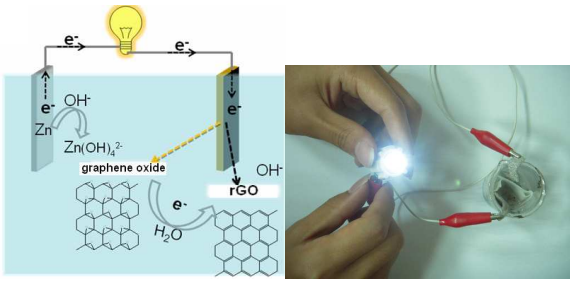

The reduction of graphene oxide by Zn can also result in power-output for Zn/GO primary cell.